Green Scheduling for Radiant Systems in Buildings*

Truong X. Nghiem, Madhur Behl, George J. Pappas and Rahul Mangharam
Department of Electrical and Systems Engineering
University of Pennsylvania
{nghiem, mbehl, pappasg, rahulm}@seas.upenn.edu

March 14, 2012

Abstract

In this report we look at the problem of peak power reduction for buildings with electric radiant floor heating systems. Uncoordinated operation of a multi-zone radiant floor heating system can result in temporally correlated electricity demand surges or peaks in the building's electricity consumption. As peak power prices are 200-400 times that of the nominal rate, this uncoordinated activity can result in high electricity costs and expensive system operation. We have previously presented green scheduling as an approach for reducing the aggregate peak power consumption in buildings while ensuring that indoor thermal comfort is always maintained. This report extends the theoretical results for general affine dynamical systems and applies them to electric radiant floor heating systems. The potential of the proposed method in reducing the peak power demand is demonstrated for a small-scale system through simulation in EnergyPlus and for a large-scale system through simulation in Matlab.

1 Introduction

Commercial electricity customers are often subject to peak-demand based electricity pricing [1]. In this pricing policy, a customer is charged not only for the amount of electricity it has consumed but also for its maximum demand over the billing cycle. The unit price of the peak demand charge is usually very high, up to 240 times in some cases [2] and even more. This is to discourage the use of electricity under peak load conditions since they can cause issues such as low quality of service and service disruptions, which affect the reliability of the grid. High peak loads also lead to a higher cost of production and distribution of electricity. Therefore, peaks in electricity usage are inefficient and expensive for both suppliers and customers.

In this report we look at the problem of peak power reduction for buildings with electric radiant floor heating systems. Uncoordinated operation of a multi-zone radiant floor heating system in a building can result in temporally correlated electricity demand surges (or peaks) leading to high electricity cost under the peak-demand pricing policy.

Radiant floor heating systems serve as an alternative to the conventional forced-air heating, ventilation and air conditioning (HVAC) systems for buildings. Radiant floor heating has been in existence for a long time but unfortunately, older buildings were not very well insulated, so high floor temperatures were required for heating, which gave floor heating a bad reputation [3]. Nowadays, these systems are widely

*This material is based upon work supported by the Greater Philadelphia Innovation Cluster (GPIC) for Energy Efficient Buildings an energy innovation HUB sponsored by the Department of Energy under Award Number DE-EE0004261.

used in both commercial and residential buildings in Korea, Germany, Austria, Denmark [4] and in some parts of the United States [3]. The benefits of radiant systems over forced-air HVAC systems for US commercial buildings has been studied in [5].

There exist several different approaches to balance the power consumption in buildings and avoid peaks, e.g., by load shifting and load shedding [6, 7]. However, they operate on coarse grained time scales and do not guarantee any thermal comfort. Another popular approach to energy efficient control for commercial buildings and data centers is model predictive control (MPC) ([8, 9, 10]). In [8] the authors investigated MPC for thermal energy storage in building cooling systems. Stochastic MPC was used to minimize building's energy consumption in [9], while peak electricity demand reduction by MPC with real-time pricing was considered in [10]. In [11] MPC is used for achieving energy savings for a hydronic central heating system.

Several improvements over the on/off control for radiant systems have been proposed in literature ([12, 13, 14, 15, 16]). Predictive control methods have been presented in [12] and [13] and are shown to improve the comfort of radiant systems. In [14], a controller called *comforstat* has been shown to improve the energy performance of a hydronic radiant heating/cooling system by regulating the water temperature. A two-parameter switching control strategy is described in [15] and is shown to achieve better temperature regulation than on/off control. In [16], three different strategies for control of multi-zone hydronic radiant systems are compared. In all of the above work, the focus has been on improving the thermal comfort of radiant floor systems by achieving better temperature regulation. *Mostly, the simulations and experimental tests have been limited to a single zone.* For the few papers that deal with radiant systems in multiple zones [13, 16], the problem of reducing the peak power, which is the focus of our work, has not been addressed.

In our recent papers [17, 18] we proposed *green scheduling* as an approach to schedule the building control systems and reduce the aggregate peak power demand while ensuring that indoor thermal comfort is always maintained. However, the results were developed for simple zone models with no thermal interactions between the zones. The contributions of this report, compared to our previous work, are threefold:

1. We extend the schedulability analysis and scheduling synthesis for general affine dynamical systems, and apply them to electric radiant floor heating systems;
2. We use a more accurate system model which incorporates the thermal dynamics of radiant heating systems, the thermal dynamics of zones, and the thermal interactions between zones;
3. We demonstrate the potential of our approach in reducing the peak demand through simulations in EnergyPlus for realistic building radiant system models.

This report is organized as follows. First, we present an overview of radiant heating systems and their dynamics, and formulate the peak demand reduction problem in Section 2. In Section 3 the generalized green scheduling problem is discussed followed by the schedulability analysis. A method for synthesizing periodic schedules for the system is proposed in Section 4. Section 5 describes two simulation case studies and shows the effectiveness of our method for reducing the peak power consumption. Finally, we conclude the report with a discussion in Section 6.

2 Radiant floor heating systems

A conventional forced-air HVAC system uses the flow of air to provide thermal comfort within a conditioned space. HVAC systems rely on ductwork, vents, etc. as means of air distribution and use air handlers, filters, blowers, heat exchangers, and various controls to regulate the temperature and flow of air entering a space.

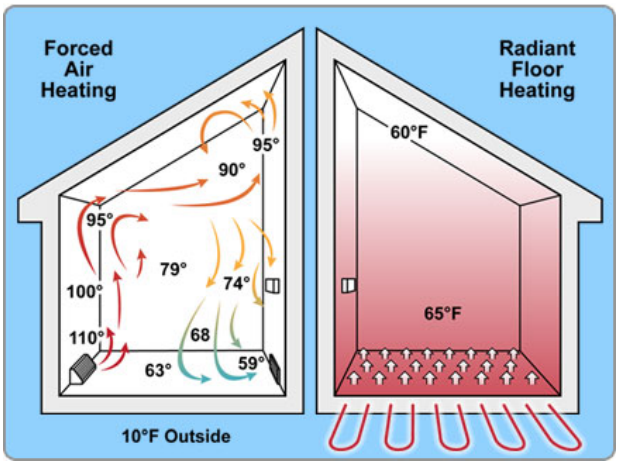

Figure 1: Comparison of air temperatures from floor to ceiling for forced-air heating (left) and radiant floor heating (right)

On the other hand, radiant heating systems involve supplying heat directly to the floor or to panels in the walls or ceiling of a house. When radiant heating is located underneath the floor, it is often called radiant floor heating (slab heating, underfloor heating or simply floor heating). A radiant floor heating system works by warming up the floor surface which then slowly radiates heat upward into the living space, rather than blowing around the heated air. This natural heat transfer is both more comfortable and energy efficient [4].

An important factor affecting building energy use and indoor comfort is thermal stratification [19]. It refers to the vertical air temperature difference that results due to the tendency of warm air rising to the ceiling and cool air settling down near the floor. As shown in Figure 1, in some situations the difference in the air temperature from floor to ceiling can exceed $20°F$ for a forced-air HVAC system. A high degree of temperature stratification leads to significantly higher air temperatures near the ceiling. This in turn increases the heat loss through the ceiling and therefore increases the heat load of the space. Radiant heating systems reduce temperature stratification and the heat loss through ceilings thus lowering the heating load. These systems also minimize drafts and dust movements, thereby providing a clean and quiet operation [20].

Modern underfloor heating systems use either electrical resistance elements or fluid flowing in pipes to heat the floor [20, 21]. Hydronic radiant floor systems pump hot water through tubing laid in a pattern underneath the floor. Electric radiant floors typically consist of electric cables (heating elements) built into the floor. Whether cables or tubing, the operation of electric and hydronic radiant systems in floors is the same. Cables or tubing are embedded within the solid floor having a high thermal capacity. If the floor's thermal mass is large enough, the thermal energy stored in it keeps the space conditioned for several hours.

2.1 Radiant floor model

We consider $m > 1$ zones. Each zone i is equipped with an electric radiant floor heating system with a maximum power rating of q_i (kW). The actuation of each radiant system is assumed to be on-off, i.e., the radiant system in each zone i can be either turned on, when it provides heating power q_i, or turned off, when it provides no heating power. Thus the control input to zone i is a binary variable $u_i \in \{0, 1\}$, where

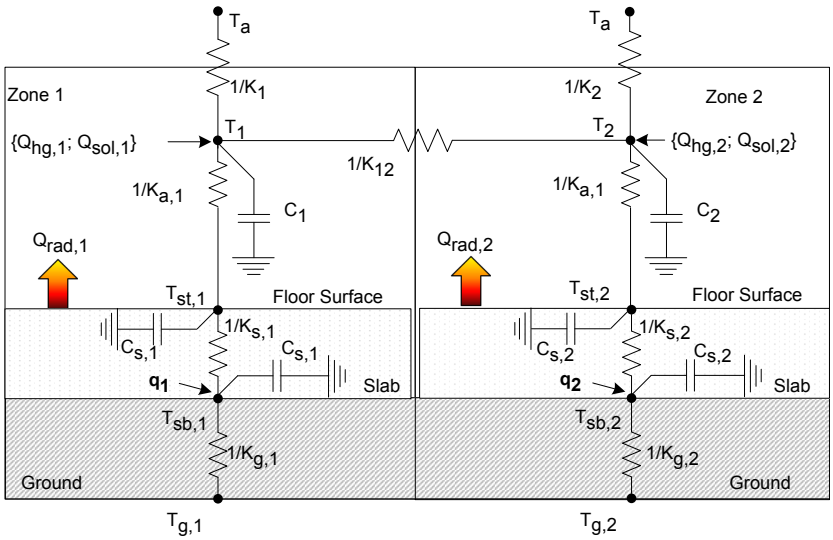

Figure 2: RC network model for an electric radiant floor heating system for 2 zones.

Table 1: List of parameters

$K_{g,i}$	conduction coefficient between ground and slab (kW/K)
$K_{a,i}$	convection coefficient between the slab and air (kW/K)
$K_{s,i}$	thermal resistance of the slab (kW/K)
$C_{s,i}$	thermal capacitance of the slab (kJ/K)
C_i	thermal capacitance of zone i (kJ/K)
K_i	thermal conductance between zone i and outside air (kW/K)
K_{ij}	thermal conductance between zone i and zone j (kW/K)

$u_i = 0$ corresponds to the off state and $u_i = 1$ the on state. The floor of each zone consists of a slab of high thermal capacity below which the radiant heat source is embedded. The dynamics of each zone is modeled using an RC network ("lumped-parameter") model as shown in Figure 2. The list of parameters in the model is given in Table 1. Each zone i has 4 nodes: $T_{g,i}$ is the ground temperature, $T_{sb,i}$ the temperature of the bottom surface of the slab, $T_{st,i}$ the temperature of the top surface of the slab, and T_i the zone air temperature (the air in the zone is assumed to be fully mixed). The heat transfer between the ground, the slab and the zone is modelled using equations of one dimensional heat conduction. This model is used by EnergyPlus [22] and was first proposed in [23]. It is assumed that the slab is uniformly heated and there is no lateral temperature difference or heat transfer. Given this model, the nodal equations for radiant system i are:

$$C_{s,i}\frac{\mathrm{d}T_{sb,i}}{\mathrm{d}t} = K_{g,i}(T_{g,i} - T_{sb,i}) + K_{s,i}(T_{st,i} - T_{sb,i}) + q_i u_i(t) \tag{1}$$

$$C_{s,i}\frac{\mathrm{d}T_{st,i}}{\mathrm{d}t} = K_{a,i}(T_i - T_{st,i}) + K_{s,i}(T_{sb,i} - T_{st,i}) \tag{2}$$

2.2 Zone model

Let T_a be the ambient air temperature (°C), which is the same for all zones. For zone i, let $Q_{hg,i}$ be its internal heat gain (kW) (from its occupants, equipments, lighting, etc.), and $Q_{sol,i}$ be the heat gain due to solar radiation (kW). We consider T_a, $Q_{hg,i}$ and $Q_{sol,i}$ as disturbances. The law of conservation of energy gives us the following heat balance equation for zone i:

$$C_i \frac{\mathrm{d}T_i(t)}{\mathrm{d}t} = K_i \left(T_a(t) - T_i(t)\right) + \sum_{j \neq i} K_{ij} \left(T_j(t) - T_i(t)\right) + K_{a,i}(T_{st,i} - T_i) + Q_{hg,i}(t) + Q_{sol,i}(t) \quad (3)$$

where C_i, K_i, and K_{ij} are parameters given in Table 1.

The differential equations (1) to (3) of the radiant floor model and the zone model for all the zones can be combined to give a state-space model of the entire system:

$$\begin{aligned} \dot{x}(t) &= Ax(t) + Bu(t) + Hw(t) \\ y(t) &= Cx(t) \end{aligned} \quad (4)$$

Here, the state vector $x = [T_{sb,1}, T_{st,1}, T_1, \ldots, T_{sb,m}, T_{st,m}, T_m]^T$ consists of the node temperatures for all zones; $u = [u_1, \ldots, u_m]^T$ is the binary control input vector to the zones; $w = [T_a, Q_{hg,1}, Q_{sol,1}, \ldots, Q_{hg,m}, Q_{sol,m}]^T$ is the vector of all disturbances; and $y = [T_1, \ldots, T_m]^T$ is the output vector of all zone air temperatures. The system is always stable, therefore state matrix A is Hurwitz.

2.3 Peak demand reduction problem

At any time t, the aggregate demand Q of all radiant heating systems is the sum of their individual power demands: $Q(t) = \sum_{i=1}^{m} q_i u_i(t)$. As mentioned in Section 1, reducing the peak demand over the billing cycle helps save energy as well as the highly priced demand charge. Thus, the objective of peak demand reduction is to minimize (or reduce) the maximum value of $Q(t)$ over a given time horizon $[0, t_f]$. However, it must also maintain the indoor thermal comfort in each zone, which requires that the air temperature T_i in zone i should be in a range $[l_i, h_i]$ (°C), e.g., between 22 °C and 24 °C. Therefore, the peak demand reduction problem can be formally stated as follows.

Problem 1 (Peak demand reduction problem): *Compute control input $u(t)$, $0 \leq t \leq t_f$, for system (4) so as to minimize the peak demand $\max_{0 \leq t \leq t_f} Q(t)$ while maintaining thermal comfort in each zone.*

In [17, 18], we described *green scheduling* to reduce the peak demand of a large number of heating systems. This was achieved by coordinating the individual systems under a constrained peak (as suggested in [24]) while ensuring that custom climate conditions are facilitated. In particular, the peak demand is restricted by requiring that at most k of the m actuators, for $1 \leq k \leq m$, can be on simultaneously. Applying the green scheduling approach to peak demand reduction for radiant heating systems results in the following problem.

Problem 2 (Green scheduling problem for radiant heating systems): *Given a peak constraint $1 \leq k \leq m$, compute control input $u(t)$, $0 \leq t \leq t_f$, for system (4) so that $\sum_{i=1}^{m} u_i(t) \leq k$ at all time while maintaining thermal comfort in each zone.*

In the next section, we generalize the green scheduling analysis results in [17, 18] to affine dynamical systems that capture the radiant system model (4). A procedure to synthesize periodic control inputs for the green scheduling problem is presented in Section 4.

3 Green scheduling for affine systems

3.1 System model for green scheduling

We first generalize the state-space model (4) of radiant heating systems for green scheduling. The disturbances w in (4) usually vary slowly. Thus, we can assume constant nominal values $\overline{w}$ for w, and adjust the model for green scheduling in real-time based on either prediction of disturbances (e.g., weather forecast, occupancy schedule) or monitoring of the environment. Therefore the system model for green scheduling is an affine dynamical model:

$$\begin{aligned} \dot{x}(t) &= Ax(t) + (Bu(t) + B_0), \quad x(0) = x_0 \\ y(t) &= Cx(t) \end{aligned} \tag{5}$$

Here, $x \in \mathbb{R}^n$ are the states, $u \in \{0,1\}^m$ the binary control inputs, $y \in \mathbb{R}^p$ the outputs, $x_0 \in \mathbb{R}^n$ the initial states. Matrix $A \in \mathbb{R}^{n \times n}$ is Hurwitz. Vector $B_0 \in \mathbb{R}^n$ corresponds to the nominal disturbances, in particular from (4) we have $B_0 = H\overline{w}$.

Operation specifications, e.g., thermal comfort, require that the outputs y should be in a *safe set* $\texttt{Safe} \subseteq \mathbb{R}^p$. `Safe` is usually a hypercube of the form $[l_1, h_1] \times \cdots \times [l_p, h_p]$, but it can also be any convex set.

A control signal $u(\cdot)$ for (5) can be thought of as a schedule that turns on-off and coordinates the individual systems. In this report, we will use the terms *control signal* and *schedule* interchangeably for $u(\cdot)$. If $u(\cdot)$ drives the system's outputs to `Safe` and maintains them in that set then the system is said to be *safe* and $u(\cdot)$ is a *safe schedule*. More precisely, the system is *safe* with $u(\cdot)$ if for any x_0, there exists a finite time $\tau \geq 0$ such that $y(t) \in \texttt{Safe}$ for all $t \geq \tau$. In the green scheduling approach the actuators u_i are coordinated so that at any time, at most k of them, for some given $1 \leq k \leq m$, can be on simultaneously. The system is said to be *k-schedulable* if there exists a safe schedule $u(\cdot)$ such that $\|u(t)\|_1 = \sum_{i=1}^m u_i(t) \leq k$ for all $t \geq 0$ (i.e., the peak constraint is always satisfied).

Our previous analysis in [17, 18] assumed that each individual system is modeled by a single state variable (which is also its output) and they are decoupled (no heat transfer between zones) so that A is diagonal. This report makes a major generalization by removing both restrictions, therefore making the model capture the actual systems more accurately.

3.2 Schedulability analysis

A fundamental question of the green scheduling problem is *k-schedulability*, that is on which conditions the system is k-schedulable for a given k. The answer to this question will allow us to find an appropriate peak constraint k. In our previous work [17, 18], k-schedulability conditions were obtained for systems with simpler dynamics by showing the existence of periodic control signals that satisfy the peak constraint and drive the system to the safe set. Along the same line, in this report, we investigate periodic control signals for system (5) to derive sufficient conditions for the system to be k-schedulable.

A T-periodic control signal u, where $T > 0$, satisfies $u(t+T) = u(t)$ for all $t \geq 0$. Define $\eta_i = \frac{1}{T}\int_0^T u_i(s)\,\mathrm{d}s \in [0,1]$ for each control input i. Because u is T-periodic, $\frac{1}{T}\int_t^{t+T} u_i(s)\,\mathrm{d}s = \eta_i$ for all $t \geq 0$. The value η_i is called the *utilization* of control input i, following the convention in real-time scheduling [25]. The utilization vector $\eta \in [0,1]^m$ of all control inputs is defined by stacking their individual utilizations, i.e., $\eta = [\eta_1, \ldots, \eta_m]^T$.

A standard tool to analyze a linear system under periodic control is its *average system*, defined as the

time-invariant affine dynamical system:

$$\begin{aligned} \dot{\overline{x}}(t) &= A\overline{x}(t) + (B_0 + B\eta)\,, \quad \overline{x}(0) = x(0) = x_0 \\ \overline{y}(t) &= C\overline{x}(t) \end{aligned} \tag{6}$$

Note that the average system starts from the same initial state and is autonomous, i.e., it does not have any input. Since A is Hurwitz, the average system is uniformly exponentially stable and converges to the unique equilibrium $\overline{x}^\star = -A^{-1}(B_0 + B\eta)$, $\overline{y}^\star = C\overline{x}^\star$. If $\overline{y}^\star$ is in the interior of `Safe`, denoted $\mathrm{int}(\texttt{Safe})$, then obviously the average system is safe. If, in addition, the output $y(t)$ of system (5) always stays close *enough* to the output $\overline{y}$ of its average system then the original system is also safe. More precisely, if there exists $\epsilon > 0$ such that

1. $\|y(t) - \overline{y}(t)\| < \epsilon$ for all $t \geq 0$; and
2. $\mathcal{B}_\epsilon(\overline{y}^\star) \subseteq \texttt{Safe}$ where $\mathcal{B}_\epsilon(\overline{y}^\star)$ denotes the open ball of radius ϵ centered at $\overline{y}^\star$

then $y(t)$ is safe. Indeed, in the next subsection, we will study the error $y(t) - \overline{y}(t)$ and show that for any $\epsilon > 0$, there exists $T > 0$ and T-periodic control signal u such that $y(t)$ is always ϵ-close to $\overline{y}(t)$.

3.2.1 State and output errors

Let $\xi(t) = x(t) - \overline{x}(t)$ and $e(t) = y(t) - \overline{y}(t) = C\xi(t)$ be respectively the state and output errors between system (5) and its average system. From (5) and (6) we obtain the dynamics of the errors:

$$\begin{aligned} \dot{\xi}(t) &= A\xi(t) + B\,(u(t) - \eta)\,, \quad \xi(0) = 0 \\ e(t) &= C\xi(t) \end{aligned} \tag{7}$$

Its solution can be written explicitly as ([26])

$$\xi(t) = \int_0^t \mathrm{e}^{A(t-s)} B\,(u(s) - \eta)\,\mathrm{d}s \tag{8}$$

at any time $t \geq 0$. Let $\sigma = \left\lfloor \frac{t}{T} \right\rfloor$, where the notation $\lfloor c \rfloor$ denotes the largest integer not exceeding c. Then we have

$$\xi(t) = \sum_{i=0}^{\sigma-1} \int_{iT}^{(i+1)T} \mathrm{e}^{A(t-s)} B\,(u(s) - \eta)\,\mathrm{d}s + \int_{\sigma T}^{t} \mathrm{e}^{A(t-s)} B\,(u(s) - \eta)\,\mathrm{d}s$$

in which the sum disappears if $\sigma = 0$ (i.e., $t < T$). We can transform the integral in the sum:

$$\int_{iT}^{(i+1)T} \mathrm{e}^{A(t-s)} B\,(u(s) - \eta)\,\mathrm{d}s = \mathrm{e}^{A(t-(i+1)T} \int_{iT}^{(i+1)T} \mathrm{e}^{A((i+1)T-s)} B\,(u(s) - \eta)\,\mathrm{d}s$$

and use the fact that u is T-periodic to obtain:

$$\begin{aligned} &= \mathrm{e}^{A(t-(i+1)T)} \int_0^T \mathrm{e}^{A(T-s)} B\,(u(s) - \eta)\,\mathrm{d}s \\ &= \mathrm{e}^{A(t-(i+1)T)} \xi_T \end{aligned}$$

in which $\xi_T = \xi(T) = \int_0^T \mathrm{e}^{A(T-s)} B\,(u(s) - \eta)\,\mathrm{d}s$. Similarly we have

$$\int_{\sigma T}^{t} \mathrm{e}^{A(t-s)} B\,(u(s) - \eta)\,\mathrm{d}s = \int_0^{t-\sigma T} \mathrm{e}^{A((t-\sigma T)-s)} B\,(u(s) - \eta)\,\mathrm{d}s = \xi(t - \sigma T)$$

Therefore,

$$\xi(t) = \left(\sum_{i=0}^{\sigma-1} \mathrm{e}^{A(t-(i+1)T)} \right) \xi_T + \xi(t - \sigma T). \tag{9}$$

Intuitively, as T gets smaller, x gets closer to $\overline{x}$ and y gets closer to $\overline{y}$. that is $\lim_{T\to 0} \|x(t) - \overline{x}(t)\| = \lim_{T\to 0} \|\xi(t)\| = 0$ for any time $t \geq 0$. Here, the symbol $\|\cdot\|$ denotes both the Euclidean vector norm and the corresponding induced matrix norm. Similarly, $\lim_{T\to 0} \|y(t) - \overline{y}(t)\| = \lim_{T\to 0} \|e(t)\| = 0$, $\forall t \geq 0$. Indeed, the following lemma gives us a *uniform* upper-bound on $\|\xi(t)\|$, *independent of time* t (its proof is given in the appendix).

Lemma 1. *There exist finite and positive constants α, β and γ, independent of u, such that for any time $t \geq 0$,*

$$\|\xi(t)\| \leq \frac{1}{2} \|A\| \gamma\beta^2 \frac{T^2}{1 - \mathrm{e}^{-\alpha T}} + \gamma\beta T.$$

Let $\|\xi\|_\infty = \sup_{t\geq 0} \|\xi(t)\|$ and $\|e\|_\infty = \sup_{t\geq 0} \|e(t)\|$ be the supremums of the point-wise distances between x and $\overline{x}$ and between y and $\overline{y}$, respectively. Then $\|\xi\|_\infty$ is bounded above by the same upper-bound in Lemma 1. By simple calculation and the l'Hôpital's rule, we can show that this upper-bound goes to 0 as $T \to 0$. The following lemma confirms the above intuition that x gets closer to $\overline{x}$ and y gets closer to $\overline{y}$ as T gets smaller.

Lemma 2. *For any T-periodic control signal u, the state and output errors between* (5) *and* (6) *go to* 0 *as T goes to* 0*, that is $\lim_{T\to 0} \|\xi\|_\infty = 0$ and $\lim_{T\to 0} \|e\|_\infty = 0$.*

Lemma 2 implies that for any $\epsilon > 0$, there exists $T_\epsilon > 0$ such that for all $0 < T \leq T_\epsilon$, any T-periodic control signal u with utilization η will drive the output y to be ϵ-close to the output $\overline{y}$ of the average system.

Remark 1: It can be proved that Lemma 1 and Lemma 2 still hold for control signals u that are not T-periodic but only satisfy the utilization constraint $\frac{1}{T}\int_{iT}^{(i+1)T} u(s)\,\mathrm{d}s = \eta$, $\forall i \in \mathbb{N}$. This enables conventional real-time scheduling algorithms [25] to be used to schedule the system. However, in this report, we only consider periodic control signals.

3.2.2 Schedulability conditions

Now that we have shown the outputs of the original system and the average system can be made arbitrarily close, we only need to construct a T-periodic control signal u such that $\|u(t)\|_1 \leq k$, $\forall t \geq 0$, to complete the schedulability analysis. It is well-known in real-time scheduling [25] that if the total utilization does not exceed k, i.e., $\sum_{i=1}^m \eta_i \leq k$, then such schedules exist.

Sufficient schedulability conditions can now be stated in the following theorem.

Theorem 3 (k-schedulability)**.** *If there exists $\eta \in [0,1]^m$ such that:*

1. $\sum_{i=1}^m \eta_i \leq k$, *and*
2. $-CA^{-1}(B_0 + B\eta) \in \mathrm{int}\,(\texttt{Safe})$,

then there exists a safe T-periodic schedule u, $T > 0$, for system (5) *such that $\|u(t)\|_1 \leq k$ for all $t \geq 0$; therefore system* (5) *is k-schedulable.*

Proof. Condition 2 implies that there exists $\epsilon > 0$ such that $\mathcal{B}_\epsilon\left(\overline{y}^\star = -CA^{-1}\left(B_0 + B\eta\right)\right) \subseteq \texttt{Safe}$. Because the average system (6) is uniformly exponentially stable with output equilibrium $\overline{y}^\star$, for any initial state x_0, there exists finite $t_{\epsilon,x_0} \geq 0$ such that $\|\overline{y}(t) - \overline{y}^\star\| < \frac{\epsilon}{2}$ for all $t \geq t_{\epsilon,x_0}$. Also, by Lemma 2, there exists $T_\epsilon > 0$ such that for any T-periodic schedule u with $0 < T \leq T_\epsilon$ and with utilization η, $\|y(t) - \overline{y}(t)\| < \frac{\epsilon}{2}$ for all $t \geq 0$, hence $y(t) \in \texttt{Safe}$ for all $t \geq t_{\epsilon,x_0}$. Condition 1 implies that there exist T-periodic schedules u satisfying $\|u(t)\|_1 \leq k$ for all $t \geq 0$. This concludes the proof. □

A similar result was derived in [27] for scheduling LQR controllers under resource constraints, however its objective is performance bound while we consider safety in this report.

3.3 Feasible peak constraint

Given system (5), it is usually of interest to find a feasible peak constraint k because k is not known at the beginning. From Theorem 3, the smallest peak constraint $k_{\min}$ can be computed by solving the optimization

$$\begin{aligned} \underset{\eta}{\text{minimize}} \quad & \sum_{i=1}^{m} \eta_i && (10) \\ \text{subject to} \quad & \eta \in [0,1]^m \\ & -CA^{-1}\left(B_0 + B\eta\right) \in \operatorname{int}\left(\texttt{Safe}\right) && (10a) \end{aligned}$$

and letting $k_{\min} = \lceil \sum_{i=1}^{m} \eta_i \rceil$, where the notation $\lceil c \rceil$ denotes the smallest integer not less than c. In practice, `Safe` is usually a hypercube or a polytope, for which constraint (10a) becomes linear and the linear programming problem (10) can be solved efficiently [28]:

- If `Safe` is a hypercube $\{y : l \leq y \leq h\}$ where $l, h \in \mathbb{R}^m$ and $l < h$ then
$$(10a) \Leftrightarrow l + CA^{-1}B_0 < -CA^{-1}B\eta < h + CA^{-1}B_0$$
- If `Safe` is a polytope $\{y : Hy \leq K\}$ where $H \in \mathbb{R}^{q \times p}$, $K \in \mathbb{R}^q$ then
$$(10a) \Leftrightarrow -HCA^{-1}B\eta < K + HCA^{-1}B_0.$$

Any peak constraint $k \geq k_{\min}$ will be feasible.

4 Periodic control synthesis

Suppose that all conditions in Theorem 3 are satisfied, thus system (5) is k-schedulable. In this section, we present a procedure to design a periodic control that both satisfies a given feasible peak constraint k and drives the system's output to `Safe`.

4.1 Limit behavior under periodic control

We first study the limit behavior of system (5) under periodic control and show that it converges to a limit cycle as $t \to \infty$. Consider some T-periodic control signal u with $T > 0$. The state error $\xi(t)$ between system (5) and its average system (6) is given in (9) and can be rewritten as

$$\xi(t) = \mathrm{e}^{A(t-\sigma T)} \left(\sum_{i=0}^{\sigma-1} \mathrm{e}^{iAT} \right) \xi_T + \xi(t - \sigma T).$$

Since A is Hurwitz, e^{AT} is Schur and therefore $\lim_{\sigma\to\infty}\sum_{i=0}^{\sigma-1}\mathrm{e}^{iAT} = \left(I-\mathrm{e}^{AT}\right)^{-1} = P$. The matrix inverse exists because the eigenvalues of $\left(I-\mathrm{e}^{AT}\right)$ are $(1-\lambda_j)$, where λ_j are eigenvalues of e^{AT}, and hence are non-zero. It follows that as $t\to\infty$, thus $\sigma = \lfloor t/T \rfloor \to \infty$, $\xi(t)$ converges to the trajectory $\hat{\xi}(t)$ given by

$$\hat{\xi}(t) = \mathrm{e}^{A(t-\sigma T)}P\xi_T + \xi(t-\sigma T). \tag{11}$$

This trajectory is a cycle because for any $t \geq 0$, $\hat{\xi}(t+T) = \mathrm{e}^{A(t-(\sigma+1)T)}P\xi_T + \xi(t-(\sigma+1)T) = \mathrm{e}^{A(t-\sigma T)}P\xi_T + \xi(t-\sigma T) = \hat{\xi}(t)$, where we use the T-periodicity of u. Furthermore, because the state $\overline{x}(t)$ of the average system converges exponentially to the equilibrium $\overline{x}^\star = -A^{-1}(B_0 + B\eta)$, $x(t) = \overline{x}(t) + \xi(t)$ converges to the limit cycle defined by $\hat{x}(t) = \overline{x}^\star + \hat{\xi}(t)$ as $t\to\infty$. Similarly, the limit cycle of $y(t)$ is given by $\hat{y}(t) = \overline{y}^\star + C\hat{\xi}(t)$ where $\overline{y}^\star = C\overline{x}^\star$.

To compute the limit cycles $\hat{x}(t)$ and $\hat{y}(t)$ for a given periodic control u, observe that $\hat{\xi}(t)$ in (11) is the solution of the ordinary differential equation (ODE)

$$\dot{\hat{\xi}}(t) = A\hat{\xi}(t) + B\left(u(t)-\eta\right), \quad \hat{\xi}(0) = P\xi_T. \tag{12}$$

Therefore, it can be computed numerically using any available ODE solver, in two steps:

1. Solve (7) for one period to compute $\xi_T = \xi(T)$;
2. Initialize $\hat{\xi}(0) = P\xi_T$ and solve (12) for one period to obtain $\hat{\xi}(t)$, $0 \leq t \leq T$.

Then the limit cycles can be computed easily.

4.2 Synthesize periodic control

In synthesizing periodic control for system (5), it is necessary to ensure that the entire limit cycle $\hat{y}(t)$ is inside `Safe`, so that the system's outputs are driven to and stay inside `Safe`. It is usually desirable to construct a periodic control signal u with the largest period T to minimize the switching frequency. Once a feasible peak constraint $k \geq k_{\min}$ is chosen (cf. Section 3.3), this is achieved by solving the optimization:

$$\begin{aligned}
\underset{\eta,T,u(\cdot)}{\text{maximize}} \quad & T \\
\text{subject to} \quad & \eta \in [0,1]^m, \quad \sum_{i=1}^{m}\eta_i \leq k, \quad T > 0 \\
& u(\cdot) \text{ is } T\text{-periodic with utilization } \eta && \text{(13a)} \\
& \|u(t)\|_1 \leq k, \forall 0 \leq t \leq T && \text{(13b)} \\
& \hat{y}(t) \in \texttt{Safe}, \forall 0 \leq t \leq T && \text{(13c)}
\end{aligned}$$

However, this optimization is difficult because $u(\cdot)$ is infinite dimensional and the limit cycle $\hat{y}(t)$ (constraint (13c)) cannot be solved analytically but only numerically. Therefore, we restrict $u(\cdot)$ to a specific form as proposed in [18], so that constraints (13a) and (13b) can be removed. We also use a search algorithm to maximize T subject to constraint (13c). Following are the steps to synthesize a periodic control with a given peak constraint $k \geq k_{\min}$.

4.2.1 Step 1: Compute utilization

Intuitively, it is desirable to have the equilibrium $\overline{y}^\star$ of the average system not only inside `Safe` but also as far as possible from the boundary of `Safe` (recall that $\hat{y}(t) = \overline{y}^\star + C\hat{\xi}(t)$). Let y_c be the Chebyshev center

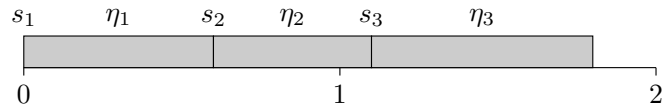

(a) Distribution of m non-overlapping intervals into $[0, k]$.

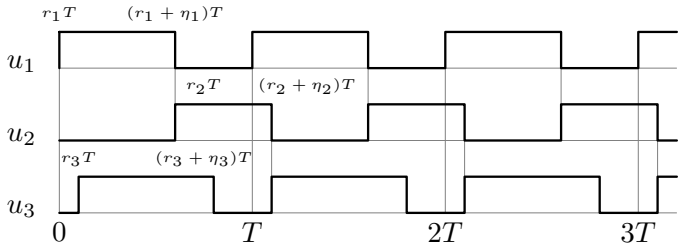

(b) Timing diagram of the constructed control input u_i from interval distribution: $r_1 = s_1$, $r_2 = s_2$, $r_3 = s_3 - 1$.

Figure 3: Construction of periodic control for $m = 3$ and $k = 2$. At any time, at most $k = 2$ control inputs are 1 simultaneously.

of `Safe`. Then η is computed by solving the following optimization:

$$\begin{aligned} \underset{\eta}{\text{minimize}} \quad & \|\overline{y}^\star - y_c\| = \left\|-CA^{-1}(B_0 + B\eta) - y_c\right\| \\ \text{subject to} \quad & \eta \in [0,1]^m, \quad \sum_{i=1}^{m} \eta_i \leq k \\ & -CA^{-1}\left(B_0 + B\eta\right) \in \operatorname{int}\left(\texttt{Safe}\right) \end{aligned}$$

where the last constraint becomes linear if `Safe` is a hypercube or a polytope.

4.2.2 Step 2: Construct periodic control

Once η has been computed, distribute m non-overlapping right-open intervals, each of length η_i respectively, into the interval $[0, k]$ on the real line (Fig. 3a). Let interval i be $[s_i, s_i + \eta_i) \subseteq [0, k]$. Since $\sum_{i=1}^{m} \eta_i \leq k$, such a distribution is always possible. Given any period $T > 0$, construct the T-periodic u_i as

$$u_i(t) = \begin{cases} 1 & \text{if } (j + r_i)\,T \leq t < (j + r_i + \eta_i)\,T,\ j \in \mathbb{N} \\ 0 & \text{otherwise} \end{cases}$$

in which $r_i = s_i - \lfloor s_i \rfloor \geq 0$. Figure 3b illustrates this construction for $m = 3$ and $k = 2$. It can be shown that $\|u(t)\|_1 \leq k$ for all t. Notice that when T varies, u keeps the same pattern and is only scaled by T in time.

4.2.3 Step 3: Compute time period T

In this step, we maximize T subject to constraint (13c), in which $\hat{y}(t)$ can only be computed numerically. T can be approximated by using a standard binary search algorithm where in each iteration, the limit cycle $\hat{y}(t)$ is computed for $t \in [0, T]$ and is checked whether it is inside `Safe`.

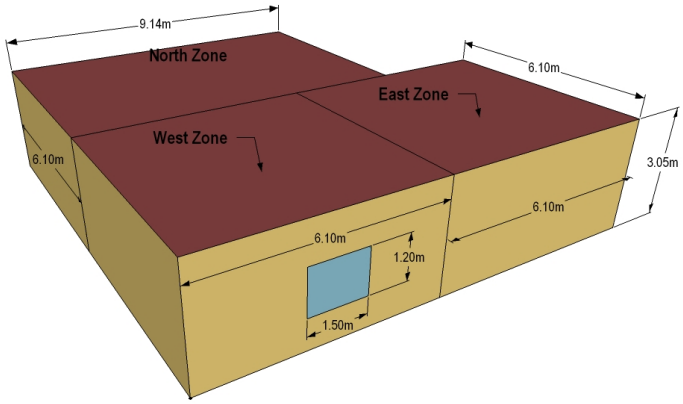

Figure 4: 3-D Building Model for the small-scale case study.

5 Case study

In this section we report the results of two case studies in which we applied the proposed green scheduling approach to multi-zone buildings with radiant heating system. We also compare the results to uncoordinated On-Off control.

5.1 Small-scale case study with EnergyPlus

In the first case study, we considered a single floor, L-shaped building divided into 3 interior conditioned zones as shown in Figure 4. There is a single window in the West zone South wall. An electric low temperature radiant system is used for heating the floor of each zone, with power ratings of 12kW, 8kW and 8kW for the North, West and East zones respectively. Temperatures in each zone were required to be kept between $l = 22\,^{\circ}\mathrm{C}$ and $h = 24\,^{\circ}\mathrm{C}$. The ambient air temperature profile was of Chicago, IL, USA. The disturbances due to internal heat gain and solar heat gain were different for every zone and time-varying.

An EnergyPlus [29] model of the building was modified from an example distributed with EnergyPlus version 7.0. In this case study, we used the EnergyPlus model as the *ground truth* for the building, i.e., it was considered as the "real" building. System identification of the building model and implementation of controllers for the building's radiant heating system were carried out in Matlab, while thermal simulation of the building was performed in EnergyPlus. We used MLE+ [30] to interface Matlab with EnergyPlus for co-simulation.

5.1.1 Model identification

Since the internal thermal model of the EnergyPlus model is not accessible from outside EnergyPlus, our first step was to identify a linear model for the building. In particular, we used the state-space model (4) developed in Section 2 and estimated its parameters based on experiment data obtained from simulation of the building in EnergyPlus. Because there are 3 zones in the building, the model has 9 state variables, 3 binary control inputs, and 3 outputs. The disturbances are the ambient air temperature, the internal heat gains for each zone, and the solar radiation for the West zone (the only zone with a window) . MLE+ and EnergyPlus were used to run controlled experiments on the building model for 5 days in January and data from EnergyPlus was recorded. The *System Identification Toolbox* [31] of Matlab was used to estimate the

building model from the experiment data.

Validation of the model was performed on January 14, which is not one of the experiment days. Figure 5 plots the measured (in EnergyPlus) and simulated (in Matlab) mean air temperatures of the zones on the validation day. The simulation outputs fit the measured outputs quite well: 84.24%, 76.89% and 84.26% for the West, East, and North zones respectively.

5.1.2 Green scheduling synthesis

We applied the green scheduling approach, described in previous sections, to the case study on the validation day. The heating schedule of the EnergyPlus model specifies that the heating system is turned off during the night from 6 PM to 6 AM, then is turned on to pre-heat the building from 6 AM to 8 AM, and is in normal operation mode from 8 AM to 6 PM (the working hours of the building). Therefore, we used green scheduling for controlling the radiant heating systems of the building from 8 AM to 6 PM.

Recall that in the system model (5) for green scheduling, we use nominal values for the disturbances. In this case study, disturbance prediction was used to derive these nominal values. According to the weather profile (Fig. 6), the ambient air temperature varied around $-5\,^{\circ}\mathrm{C}$ between 8 AM and 6 PM, thus we used $-5\,^{\circ}\mathrm{C}$ as the nominal value for T_a. Based on the occupancy and equipment schedules, the internal heat gain of each zone can be predicted, and we chose its nominal value to be 600 W, 700 W, and 800 W for the West, East, and North zones respectively. For the predicted solar radiation gain to the West zone (the only zone with a window), we noticed a significant increase at around 1 PM due to the window's direction, from under 200 W to over 1000 W (Fig. 7). Therefore, we chose two different nominal solar radiation gains: 100 W before 1 PM and 600 W after 1 PM (both were averaged values for the respective intervals).

On inspecting the predicted disturbances, we decided to synthesize two periodic schedules: one to be used before 1 PM and one after 1 PM. Their parameters are reported in Table 2. Notice that the time period T were both 60 minutes, which are reasonably large. Total computation time was less than 1 s for each case. Because the computation is fast, instead of using disturbance prediction, we could monitor the environment (e.g., ambient air temperature, occupancy) and regenerate the schedule on the fly whenever there is a significant change in the disturbances.

Schedule	k	η	T (minutes)	Nominal disturbances
Before 1 PM	2	$[0.35, 0.42, 0.45]$	60	$\overline{T}_a = -5\,^{\circ}\mathrm{C}$, $\overline{Q}_{hg,\mathrm{west}} = 600\,\mathrm{W}$, $\overline{Q}_{hg,\mathrm{east}} = 700\,\mathrm{W}$, $\overline{Q}_{hg,\mathrm{north}} = 800\,\mathrm{W}$, $\overline{Q}_{sol,\mathrm{west}} = 100\,\mathrm{W}$
After 1 PM	1	$[0.05, 0.19, 0.31]$	60	$\overline{T}_a = -5\,^{\circ}\mathrm{C}$, $\overline{Q}_{hg,\mathrm{west}} = 600\,\mathrm{W}$, $\overline{Q}_{hg,\mathrm{east}} = 700\,\mathrm{W}$, $\overline{Q}_{hg,\mathrm{north}} = 800\,\mathrm{W}$, $\overline{Q}_{sol,\mathrm{west}} = 600\,\mathrm{W}$

Table 2: Two periodic schedules for the small-scale case study

5.1.3 Simulation results

The periodic schedules were implemented in Matlab and interfaced with the building energy simulation in EnergyPlus via MLE+. For comparison, we also implemented the uncoordinated on-off control strategy, where the radiant system in each zone was controlled by an individual two-position thermostat. The thermostats worked independently of each other. Zone temperatures from the simulations are plotted in Fig. 8. In both cases, zone temperatures were kept in the desired range between $22\,^{\circ}\mathrm{C}$ and $24\,^{\circ}\mathrm{C}$. We observed that the curve of electricity demand for the uncoordinated control strategy had several high

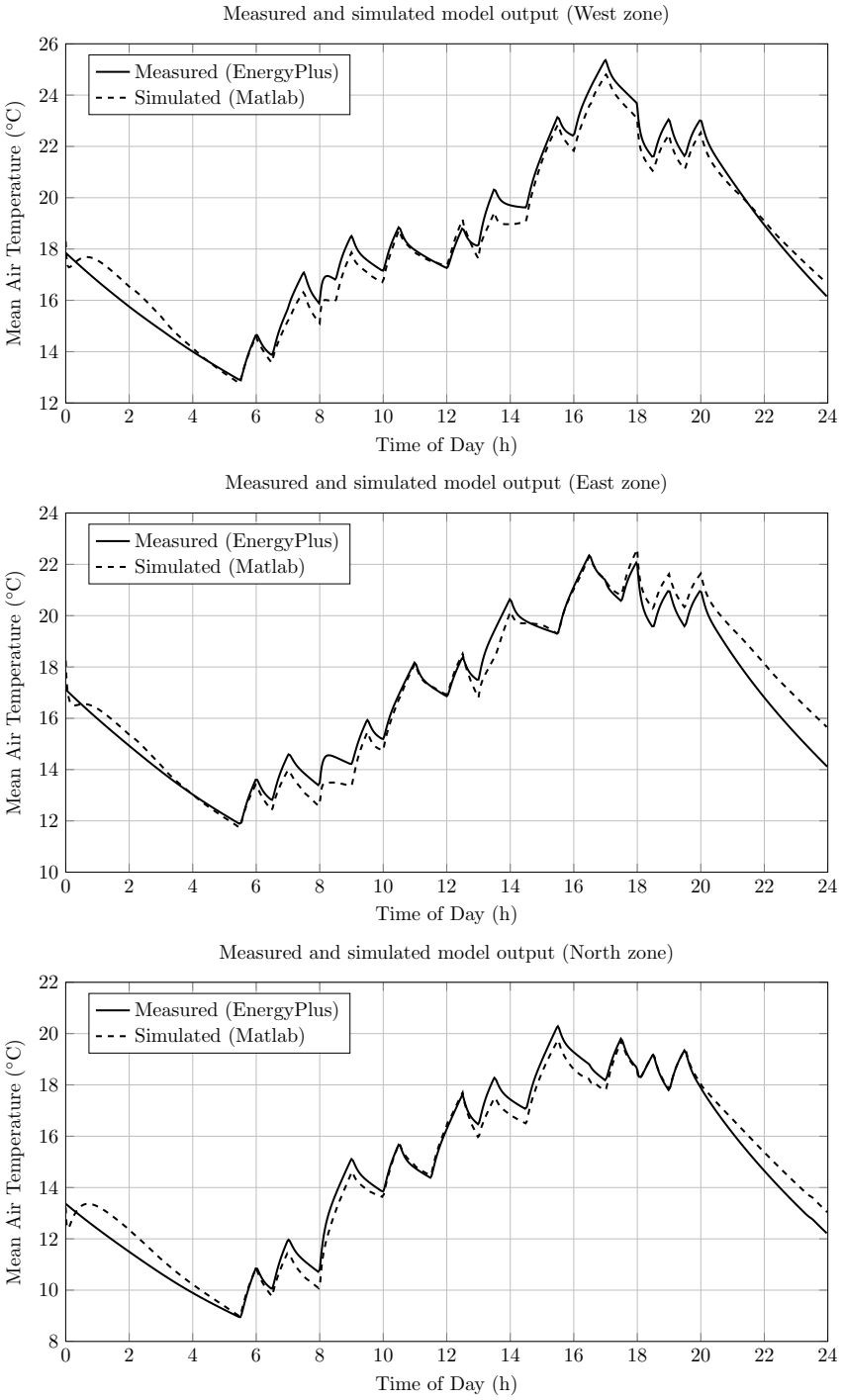

Figure 5: Validation of the identified model in the small-scale case study.

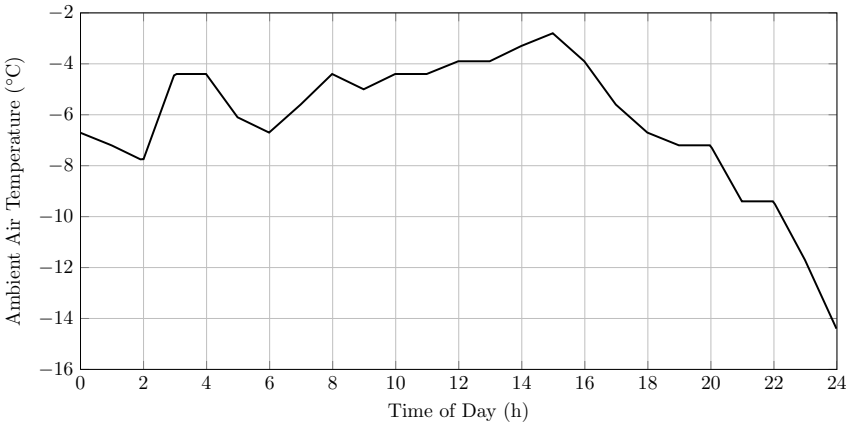

Figure 6: Ambient air temperature profile in the small-scale case study.

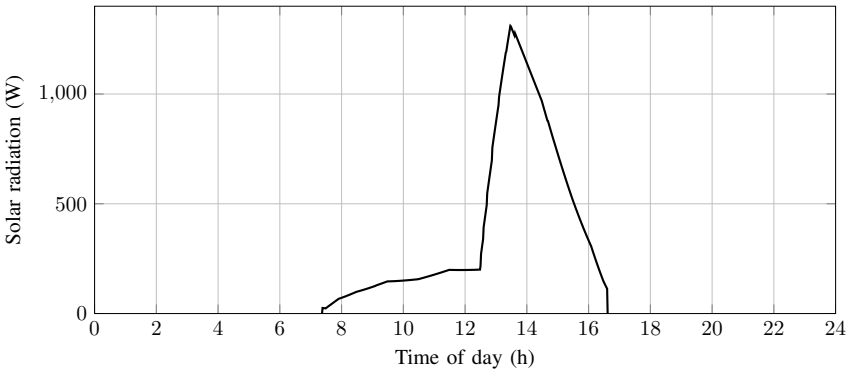

Figure 7: Predicted solar radiation gain to the West zone in the small-scale case study.

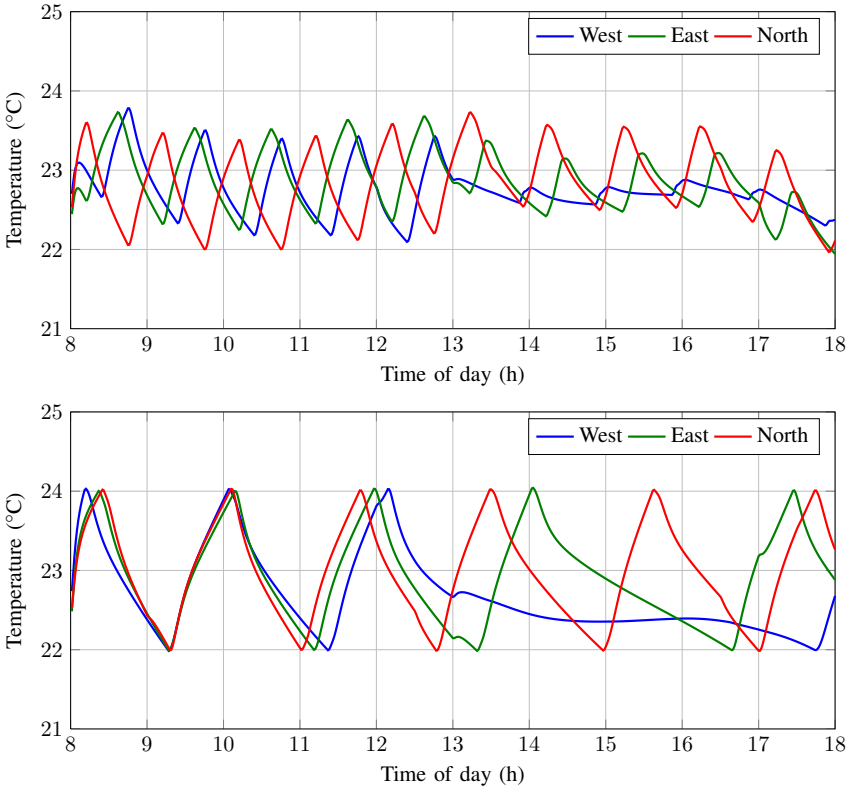

Figure 8: Zone temperatures for green scheduling (top) and uncoordinated on-off control (bottom) in the small-scale case study.

spikes (or peaks) while it was more smooth and flat for the green scheduling strategy (Fig. 9). For green scheduling, the effect of switching from the first schedule (peak constraint $k = 2$) to the second schedule (peak constraint $k = 1$) at 1 PM can be seen clearly in Fig. 8 and Fig. 9. In total, green scheduling helped save 8% in electricity consumption and reduce peak demand by 42.9% (Table 3). This result showed the potential of the proposed approach for reducing peak energy demand. There is a decrease in the total energy consumption since the periodic schedule tends to operate at a lower mean temperature than uncoordinated control (Fig. 8).

	Uncoordinated	Green scheduling (% saved)
Consumption (kW h)	93.2	85.7 (8.0%)
Peak demand (kW)	28.0	16.0 (42.9%)

Table 3: Peak demand and consumption in the small-scale case study

5.2 Large-scale case study

We have seen in the small-scale case study that green scheduling helped reduce peak demand and flatten the demand curve. The advantage of green scheduling will be displayed more clearly when there are a large number of systems to be coordinated. In this case study, we took the linear model in the first case study

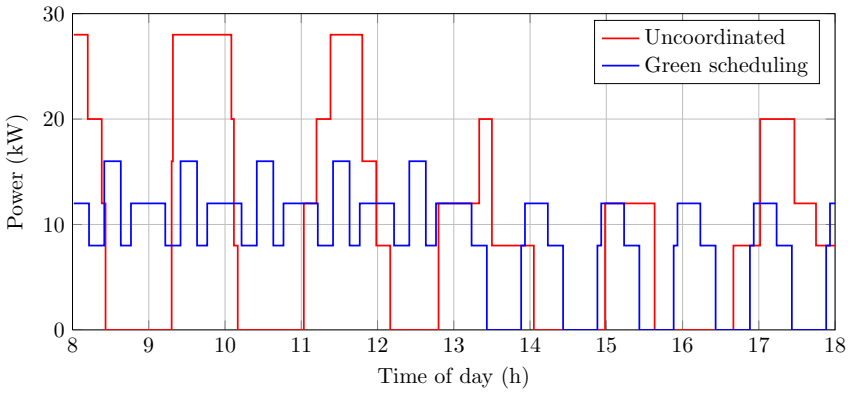

Figure 9: Electricity demands in the small-scale case study.

and scaled it to 100 zones. The zones were still coupled, i.e., there were thermal interactions between them. However, unlike the first case study, we simulated the thermal model only in Matlab, not in EnergyPlus because an EnergyPlus model was not available.

Using the same green scheduling synthesis, the peak constraint was computed to be $k = 51$ (among 100) and the time period T was again 60 minutes. The computation in Matlab took only about 3 seconds to complete. We implemented both the green scheduling and the uncoordinated on-off control for comparison. As can be seen on the electricity demand plots in Fig. 10, the demand curve of the green scheduling was almost flat with no sudden spikes, while that of the uncoordinated control had very high peaks repeatedly. Electricity consumption and peak demand are reported in Table 4. In total, green scheduling saved 5.15% in electricity consumption and 32.41% in peak demand, compared to uncoordinated control.

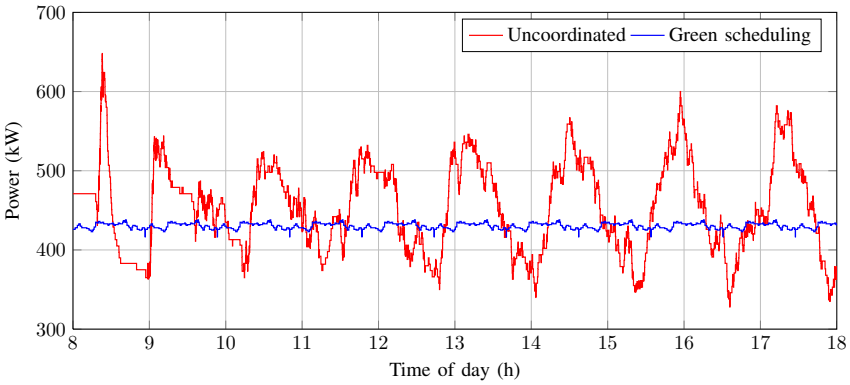

Figure 10: Electricity demands in the large-scale case study.

	Uncoordinated	Green scheduling (% saved)
Consumption (kW h)	4536.8	4303.3 (5.15%)
Peak demand (kW)	648.0	438.0 (32.41%)

Table 4: Peak demand and consumption in the large-scale case study

6 Conclusion

The green scheduling approach for peak power reduction in buildings has been extended to work with electric radiant floor heating systems. The model used in this report captures the dynamics of actual systems more accurately than in our previous work. We derived sufficient schedulability conditions for general affine dynamical systems and proposed a method for synthesizing periodic schedules for them. Through realistic simulations in EnergyPlus, we showed that our approach is effective for reducing the peak demand of a multi-zone radiant floor heating system while ensuring that the desired thermal comfort level in each zone is maintained. The approach was also shown to be scalable for a large number of zones. Lowering the peak power consumption of these systems has large economic benefits due to peak-demand based electricity pricing policies.

The fast computation time of our method, e.g., about 3 seconds for 100 zones in our case study, allows us to deal with time varying disturbances by recomputing the schedule on the fly when the disturbances change significantly. Since the control signal is on/off, the frequency of switching of the radiant system equipments becomes an important concern. The switching rate depends on how fast the dynamics of the system are and can be controlled. In our case studies, the switching rates were reasonably large (once every hour).

In this work, the thermal inputs to the system were selected from a discrete set, i.e., the control signal (schedule) was only on/off. However, many modern radiant heating systems provide more continuous control options. For future work, we want to look at incorporating continuous control inputs in green scheduling. Hierarchical scheduling algorithms for peak power reduction in an extremely large-scale system with several buildings, each with multiple zones, will be considered. We are also investigating state-feedback dynamic scheduling algorithms and schedules based on dynamic pricing models that can lead to peak power reduction in a more on-line fashion. Our current efforts are on building a test-bed for radiant floor heating system to evaluate and validate the performance of our method.

Disclaimer

References

[1] M. H. Albadi and E. F. El-Saadany, "Demand response in electricity markets: An overview," in *Proc. IEEE Power Engineering Society General Meeting*, 2007, pp. 1–5.

[2] TRFund Energy Study, "Understanding PECO's general service tariff," 2007.

[3] B. I. Doebber, M. Moore, and M. Deru, "Radiant slab cooling for retail," *ASHRAE Journal*, vol. 52, no. December, pp. 28+, 2010.

[4] B. Olesen, "Radiant floor heating in theory and practice," *ASHRAE Journal*, vol. 44, no. 7, pp. 19–24, 2002.

[5] Corina and Stetiu, "Energy and peak power savings potential of radiant cooling systems in US commercial buildings," *Energy and Buildings*, vol. 30, no. 2, pp. 127 – 138, 1999.

[6] S. Kiliccote, M. Piette, and D. Hansen, "Advanced controls and communications for demand response and energy efficiency in commercial buildings," in *Second Carnegie Mellon Conf. in Elec. Power Sys.*, 2006.

[7] K. ho Lee and J. E. Braun, "Development of methods for determining demand-limiting setpoint trajectories in buildings using short-term measurements," *Building and Environment*, vol. 43, no. 10, pp. 1755 – 1768, 2008.

[8] Y. Ma, F. Borrelli, B. Hencey, B. Coffey, S. Bengea, and P. Haves, "Model predictive control for the operation of building cooling systems," in *Proc. ACC'10*, 2010, pp. 5106–5111.

[9] F. Oldewurtel, A. Parisio, C. N. Jones, M. Morari, D. Gyalistras, M. Gwerder, V. Stauch, B. Lehmann, and K. Wirth, "Energy efficient building climate control using stochastic model predictive control and weather predictions," in *Proc. ACC'10*, Jun. 2010, pp. 5100 –5105.

[10] F. Oldewurtel, A. Ulbig, A. Parisio, G. Andersson, and M. Morari, "Reducing peak electricity demand in building climate control using real-time pricing and model predictive control," in *Proc. IEEE CDC'10*, 2010, pp. 1927–1932.

[11] F. Tahersima, J. Stoustrup, and H. Rasmussen, "Optimal power consumption in a central heating system with geothermal heat pump," in *Proc. of the 18th IFAC World Congress*. IFAC, 2011.

[12] T.Y. and Chen, "Application of adaptive predictive control to a floor heating system with a large thermal lag," *Energy and Buildings*, vol. 34, no. 1, pp. 45 – 51, 2002.

[13] J.-Y. Lee, M.-S. Yeo, and K.-W. Kim, "Predictive control of the radiant floor heating system in apartment buildings," *Journal of Asian Architecture and Building Eng.*, vol. 1, no. 1, pp. 105–112, 2002.

[14] A. Beghi, L. Cecchinato, and M. Rampazzo, "Thermal and comfort control for radiant heating/cooling systems," in *2011 IEEE Int. Conf. on Control Applications*, Sept. 2011, pp. 258 –263.

[15] S.-H. Cho and M. Zaheer-uddin, "An experimental study of multiple parameter switching control for radiant floor heating systems," *Energy*, vol. 24, no. 5, pp. 433 – 444, 1999.

[16] P. Gibbs, "Control of multizone hydronic radiant floor heating system." *ASHRAE Transactions: Part 1*, pp. 1003–1010, 1994.

[17] T. X. Nghiem, M. Behl, R. Mangharam, and G. J. Pappas, "Green scheduling of control systems for peak demand reduction," in *IEEE Conference on Decision and Control (CDC 2011)*, December 2011.

[18] ——, "Scalable scheduling of building control systems for peak demand reduction," in *American Control Conferencee*, Montreal, Canada, June 2012.

[19] ASHRAE, *ANSI/ASHRAE Standard 55-2004, Thermal Comfort Conditions for Human Occupancy.* American Society of Heating, Air-Conditioning, and Refrigeration Engineers, Inc., 2004.

[20] J. Siegenthaler, *Modern Hydronic Heating: For Residential and Light Commercial Buildings.* Cengage Learning, 2011.

[21] ASHRAE, *2008 ASHRAE Handbook - Heating, Ventilating, and Air-Conditioning Systems and Equipment*, ser. ASHRAE Handbook. ASHRAE, 2008.

[22] *EnergyPlus Engineering Reference: The Reference to EnergyPlus Calculations*, Oct. 2011.

[23] J. Seem, *Modeling of heat transfer in buildings*. University of Wisconsin–Madison, 1987.

[24] ASHRAE, *HVAC Applications*, ser. ASHRAE Handbook. Atlanta, GA: ASHRAE, 2007, ch. 41, p. 41.36.

[25] J. W. S. Liu, *Real-time Systems*. Prentice Hall, 2000.

[26] W. J. Rugh, *Linear System Theory*, 2nd ed. Upper Saddle River, NJ, USA: Prentice-Hall, Inc., 1996.

[27] J. Le Ny, E. Feron, and G. J. Pappas, "Resource constrained LQR control under fast sampling," in *Proc. of HSCC '11*. ACM, 2011, pp. 271–280.

[28] S. Boyd and L. Vandenberghe, *Convex Optimization*, 1st ed. Cambridge University Press, 2006.

[29] B. D. B. Crawley and L. K. Lawrie, "Energyplus : Energy simulation program," *Manager*, vol. 42, no. 4, pp. 49–56, 2000.

[30] T. X. Nghiem, "MLE+: a Matlab-EnergyPlus co-simulation interface," http://www.seas.upenn.edu/~nghiem/mleplus.html.

[31] The MathWorks, "System identification toolbox," http://www.mathworks.com/products/sysid.

Appendices

A Proof of Lemma 1

Because state matrix A is Hurwitz, there exist positive constants α, β such that $\left\|\mathrm{e}^{At}\right\| \leq \beta \mathrm{e}^{-\alpha t}$ for all $t \geq 0$. It follows from (9) that for any $t \geq 0$,

$$\begin{aligned}\|\xi(t)\| &= \left\| \left(\sum_{i=0}^{\sigma-1} \mathrm{e}^{A(t-(i+1)T)} \right) \xi_T + \xi(t-\sigma T) \right\| \\ &\leq \left(\sum_{i=0}^{\sigma-1} \left\| \mathrm{e}^{A(t-(i+1)T)} \right\| \right) \|\xi_T\| + \|\xi(t-\sigma T)\| \end{aligned} \tag{14}$$

The matrix norm in the sum is bounded by $\left\|\mathrm{e}^{A(t-(i+1)T)}\right\| \leq \beta \mathrm{e}^{-\alpha(t-(i+1)T)}$. Therefore,

$$\sum_{i=0}^{\sigma-1} \left\| \mathrm{e}^{A(t-(i+1)T)} \right\| \leq \beta \sum_{i=0}^{\sigma-1} \mathrm{e}^{-\alpha(t-(i+1)T)} = \beta \mathrm{e}^{-\alpha(t-\sigma T)} \sum_{i=0}^{\sigma-1} \mathrm{e}^{-i\alpha T}$$

where $\mathrm{e}^{-\alpha(t-\sigma T)} \leq 1$ since $t \leq \sigma T$, hence

$$\sum_{i=0}^{\sigma-1} \left\| \mathrm{e}^{A(t-(i+1)T)} \right\| \leq \beta \frac{1-\mathrm{e}^{-\sigma\alpha T}}{1-\mathrm{e}^{-\alpha T}} \leq \beta \frac{1}{1-\mathrm{e}^{-\alpha T}}. \tag{15}$$

From (8) we have

$$\xi(t-\sigma T) = \int_0^{t-\sigma T} \mathrm{e}^{A((t-\sigma T)-s)} B\left(u(s)-\eta\right) \mathrm{d}s.$$

Consider the term $B\left(u(s)-\eta\right)$. Because $u(s)$ is a binary vector of length m, there are only a finite number of possible values of $u(s)$. It follows that $\|B\left(u(s)-\eta\right)\|$ is bounded above by some finite constant γ, that is $\|B\left(u(s)-\eta\right)\| \leq \gamma$ for all $s \geq 0$. The last term in (14) can then be bounded by:

$$\begin{aligned}
\|\xi(t-\sigma T)\| &\leq \int_0^{t-\sigma T} \left\|\mathrm{e}^{A((t-\sigma T)-s)}\right\| \|B\left(u(s)-\eta\right)\| \,\mathrm{d}s \\
&\leq \gamma\beta \int_0^{t-\sigma T} \mathrm{e}^{-\alpha((t-\sigma T)-s)} \,\mathrm{d}s \\
&= \frac{\gamma\beta}{\alpha}\left(1-\mathrm{e}^{-\alpha(t-\sigma T)}\right) \\
&\leq \frac{\gamma\beta}{\alpha}\alpha\left(t-\sigma T\right) \\
&\leq \gamma\beta T
\end{aligned} \tag{16}$$

in which we use the inequality $1-\mathrm{e}^{-x} \leq x$ for $x \geq 0$, and the fact that $0 \leq t-\sigma T < T$.

The same bound could have been used for $\|\xi_T\|$, however it would make the bound in (14) not go to 0 as $T \to 0$, which is undesirable. A better bound for $\|\xi_T\|$ can be achieved by rewriting ξ_T as:

$$\begin{aligned}
\xi_T &= \int_0^T \mathrm{e}^{A(T-s)} B\left(u(s)-\eta\right) \mathrm{d}s \\
&= \int_0^T \left(\mathrm{e}^{A(T-s)} - I\right) B\left(u(s)-\eta\right) \mathrm{d}s + B\int_0^T \left(u(s)-\eta\right) \mathrm{d}s
\end{aligned}$$

and noting that $\int_0^T \left(u(s)-\eta\right) \mathrm{d}s = 0$ by definition, and that $\mathrm{e}^{A(T-s)} - I = \left(\int_0^{T-s} \mathrm{e}^{Av} \,\mathrm{d}v\right) A$, hence

$$= \int_0^T \left(\int_0^{T-s} \mathrm{e}^{Av} \,\mathrm{d}v\right) AB\left(u(s)-\eta\right) \mathrm{d}s.$$

We have that

$$\left\|\int_0^{T-s} \mathrm{e}^{Av} \,\mathrm{d}v\right\| \leq \int_0^{T-s} \left\|\mathrm{e}^{Av}\right\| \mathrm{d}v \leq \beta\int_0^{T-s} \mathrm{e}^{-\alpha v} \,\mathrm{d}v = \frac{\beta}{\alpha}\left(1-\mathrm{e}^{-\alpha(T-s)}\right) \leq \beta(T-s).$$

Therefore,

$$\|\xi_T\| \leq \int_0^T \left\|\int_0^{T-s} \mathrm{e}^{Av} \,\mathrm{d}v\right\| \|A\| \|B\left(u(s)-\eta\right)\| \,\mathrm{d}s \leq \|A\|\gamma\beta\int_0^T (T-s) \,\mathrm{d}s = \frac{1}{2}\|A\|\gamma\beta T^2. \tag{17}$$

Combining bounds (14) to (17) gives us the upper-bound in Lemma 1.